



Article

A Critical Comparison of the Cuk and the Sheppard–Taylor Converter

Alfredo Alvarez-Diazcomas ¹, Juvenal Rodríguez-Reséndiz ^{1,*}, Roberto V. Carrillo-Serrano ¹,
Adyr A. Estévez-Bén ² and José Manuel Álvarez-Alvarado ¹

¹ Facultad de Ingeniería, Universidad Autónoma de Querétaro, Las Campanas, Querétaro 76010, Mexico

² Facultad de Química, Universidad Autónoma de Querétaro, Las Campanas, Querétaro 76010, Mexico; aestevz05@alumnos.uaq.mx

* Correspondence: juvenal@uaq.edu.mx

Abstract: The use of and interest in renewable energy have increased in recent years due to the environmental impact of the technologies currently used to generate electricity. Switched converters play a fundamental role in renewable energy systems. The main goal is to manipulate the output signal of the renewable energy source to meet the requirements of different loads. Therefore, the increase in research on renewable energy sources has resulted in an increase in studies on switched converters. However, many DC–DC converters can be used in a particular application, and there is no clear guidance on which converter to use. The choice of whether to use one converter over another is highly reliant on the expertise of the researcher. Two examples of DC–DC converters are the Sheppard–Taylor converter and the Cuk converter. In this work, a critical comparison is made between these converters. The parameters considered in this comparison are the number of components, gain, stress on parts, and others. The simulation results were obtained to evaluate the performance of the converters in different scenarios. Finally, we conclude that the only application for which the use of the Sheppard–Taylor converter is justified are those that require high specific power and power density.

Keywords: DC–DC converter; Sheppard–Taylor converter; Cuk converter; modeling converters



Citation: Alvarez-Diazcomas, A.; Rodríguez-Reséndiz, J.; Carrillo-Serrano, R.V.; Estévez-Bén, A.A.; Álvarez-Alvarado, J.M. A Critical Comparison of the Cuk and the Sheppard–Taylor Converter. *World Electr. Veh. J.* **2023**, *14*, 148. <https://doi.org/10.3390/wevj14060148>

Academic Editor: Hang Gao

Received: 1 March 2023

Revised: 26 May 2023

Accepted: 1 June 2023

Published: 4 June 2023



Copyright: © 2023 by the authors. Licensee MDPI, Basel, Switzerland. This article is an open access article distributed under the terms and conditions of the Creative Commons Attribution (CC BY) license (<https://creativecommons.org/licenses/by/4.0/>).

1. Introduction

The use of renewable energy sources has significantly increased in recent decades. This increase is mainly due to the large number of greenhouse gases emitted into the atmosphere by traditional energy sources. In addition, international agreements to reduce the environmental impact of power generation have been established, such as the Kyoto protocol. Therefore, there are significant projects related to clean energy generation in almost every country [1,2]. According to the 2020 global status report of REN21, it is cheaper to generate power from solar panels than build new coal plants in most countries. The installed capacity of renewable energies in 2019 grew by more than 200 GW due to this cost reduction. This growth represents the highest growth in installed capacity for a single year. In addition, renewable energies provided 27.3% of the total energy consumed globally in 2019 [3].

Switched converters play a crucial role in power generation systems based on renewable energy sources. The source must often operate at a specific point to provide the maximum power. The extracted energy can be sent to a battery for storage, from which it can be directly injected into the grid or consumed locally. All loads have different voltage and current requirements that must be met by the system to ensure proper operation. Switched converters can manipulate the source output signals of the signals input to the load. Hence, they allow the source to operate at its maximum power transfer point while meeting the load requirements. Hence, along with the increase in renewable energy sources, the use of switched converters has also correspondingly increased [4,5].

Another factor that has driven the branch of power electronics is technological advancement. Metal oxide silicon field-effect transistors (MOSFETs) appeared in the industry in the 1970s. Since then, they have continued to evolve to meet the growing demands of electricity in our daily lives. However, the rate of improvement of silicon-based devices has declined this century, as they almost reached their maximum theoretical capabilities. However, innovative wide-bandgap materials have been introduced, such as silicon carbide (SiC) and gallium nitride (GaN). GaN and SiC semiconductor materials allow for the production of faster, smaller, and more reliable devices. Moreover, the efficiency of devices with this new technology is superior to that of traditional silicon-based solutions. These capabilities allow power converters to be used in a wide range of applications, which was not possible with the previous technology [6,7]. Therefore, it is essential to increase research efforts associated with power converters.

There are many types of power converters. These converters can be classified according to the current type at the input and output (DC–DC, DC–AC, AC–DC, and AC–AC). Generally, DC–DC converters have a variable DC voltage at their input and a fixed DC voltage at their output. These converters are very common in renewable energy source applications. The most basic DC–DC converter topologies are the buck and boost converters [8–10]. However, there are many other types of DC–DC converter topologies, such as in the examples of the Sheppard–Taylor and Cuk converters.

Figure 1 shows the Cuk converter topology. This type of converter was first proposed by researcher Slobodan Cuk in 1977 [11]. Since its invention, this converter has been the basis of much research. Performing a search for Cuk converter in the title, abstract, and keywords using the Scopus tool resulted in 1602 items. In addition, since 2017, more than 100 articles per year have been published in relation to this converter. Furthermore, it has been used in a wide range of applications. In [12], a study was carried out comparing the classic boost converter with the Cuk. The Cuk converter was found to present significant advantages for voltage boost applications, because it is more efficient and has less ripple at the output. In [13], this converter was used to obtain an IV curve in a photovoltaic array. Advantages of the architecture were demonstrated in allowing automation in the process of characterizing a photovoltaic panel. In [14], a modified Cuk converter was proposed for telecommunications applications, with a lower ripple for the output current, and a higher output voltage was achieved. In [15,16], the Cuk converter was combined with a classic boost topology for renewable energy applications. In both works, control of the cascade converter was achieved using a single control signal to a switch. The results show that it is possible to work in the MPPT with a low stress level on the switches, and a higher voltage gain at the output was obtained compared with classical topologies. Finally, Refs. [17,18] used the Cuk converter for power factor correction (PFC). It was used as a battery charger for an electric vehicle in one and as a driver for a motor in the other. The effectiveness of using this converter in a battery charger was evidenced even under conditions of line voltage and load variations. Moreover, very low ripple regulation in the output voltage was maintained, which is highly desirable in battery charger applications. On the other hand, when used as a motor driver, it was shown that the power factor tends to be one, and the total harmonic distortion (THD) of the supply current is reduced for low-power applications. As can be seen, this converter is used in a wide range of applications; therefore, it demonstrates great potential both presently and in the future.

Figure 2 shows the Sheppard–Taylor converter architecture. This converter was proposed in 1983 [19]. When performing a search for Sheppard–Taylor converter in the title, abstract, and keywords using the Scopus tool, 51 articles were returned. The difference between both converters is huge. However, the Sheppard–Taylor converter has been used in numerous applications. These include DC motor drivers [20,21] and battery chargers [22,23]. However, most applications are related to power factor correction (PFC). Despite the significant difference, many works on the applications of this architecture can be analyzed. However, the vast majority are related to PFC applications. Some examples are [20,22,23], among others. The reason this topology is so popular for PFC is due to two

main reasons; according to [24], this converter achieves a high power factor when operated in discontinuous mode for a wide range of operations and can achieve a perfect sine input current when working in continuous mode.

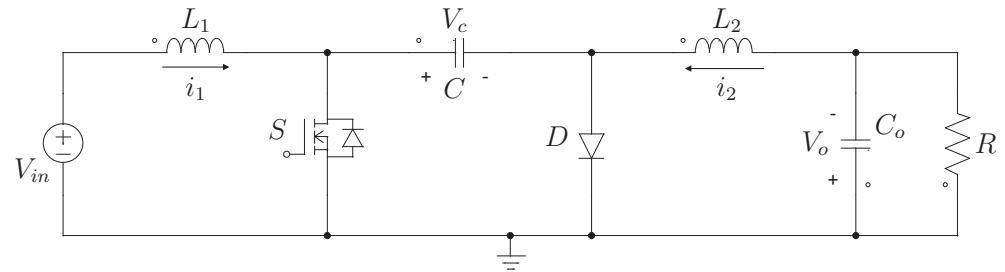


Figure 1. Cuk converter topology.

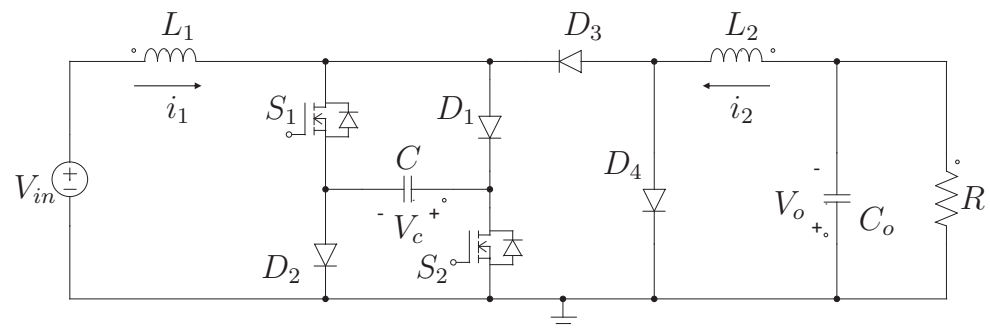


Figure 2. Architecture of the Sheppard–Taylor converter.

By analyzing Figures 1 and 2, it can be seen that both converters have many characteristics in common. Both have inductors at the input and output stages to regulate the current. In addition, they each have one capacitor between the input and the output phases. Finally, the negative terminal of the input source is directly connected to the positive terminal of the output capacitor. However, despite all these common features, there is a vast difference in the research between both converters. At first sight, it can be appreciated that the Cuk converter uses fewer components. Nevertheless, is that reason enough to justify the difference in their use? Is the Sheppard–Taylor converter superior to the Cuk converter applications not related to PFC? We attempt to answer these questions in the present work.

There are many reviews and comparisons of DC–DC converters [25–27]. However, we have only found two articles that include both Sheppard–Taylor and Cuk converters [28,29]. In [28], a unified approach was proposed to analyze PFC converters. The authors focused on a methodology to analyze the behavior and design of both converters. However, a proper comparison between both converters was not performed. On the other hand, in [29], both converters were used as drivers for a DC motor and focused on the performance of an electric machine. It remains to be found why the Cuk converter is used much more than the Sheppard–Taylor converter. Therefore, this work performs an in-depth study comparing both converters. We hope the results presented here can justify why the Cuk converter is more frequently used. Moreover, we intend to give future designers guidelines for when to use the Sheppard–Taylor converter. Table 1 presents some of the most recent works that involve the converters discussed in this manuscript and their contribution to the study area.

Table 1. Use of Cuk and Sheppard–Taylor converters in investigations of the area.

Reference/Year	Contribution to the Field of Study
[30]	In this paper, a flicker-free LED driver based on an isolated Cuk converter with integrated magnetic technique is proposed. Two inductors and a power transformer are combined into one magnetic core to eliminate the wave current as much as possible.
[31]	In this study is an optimized on-board integrated DC/DC converter with a non-isolated multi-port scheme that integrates a unidirectional port for the fuel cell and a bidirectional port for the battery and load. This can achieve combined energy supply and recovery with a single integrated converter, effectively overcoming the above disadvantages.
[32]	The authors perform an improved bidirectional Cuk equalizer (BCEQ) structure based on a variable-domain fuzzy PID (VFPID) control equalization strategy which is recommended in stages.
[33]	This paper deals with the design and analysis of a power factor correction-based Sheppard–Taylor converter-fed brushless DC motor (BLDCM) drive.
[34]	This paper proposes a high-gain Sheppard–Taylor-fed electric vehicle in a grid-connected PV system. The Sheppard–Taylor converter is used to maintain the voltage of solar panels at a constant. The output of this Sheppard–Taylor converter is maintained at a constant with the assistance of the PI controller.

In this paper, we compare two DC–DC converters: the Sheppard–Taylor converter and the Cuk converter. This comparison is conducted considering the number of components, voltage gain, converter model, stress on components, and other parameters. Therefore, in this work, we offer the key points that differentiate these topologies such that a future designer can decide which converter to use in their application. Section 2 presents the model of both converters. Section 3 presents the simulation results for several scenarios of these converters, and Section 4 offers a critical comparison between these converters considering the parameters mentioned above. Finally, the main deductions of the investigation are presented in the conclusions.

2. Modeling of the Converters

In this section, an averaged model of each converter is developed. The application of the averaged model is a well-known technique used for switched converters [35]. By modeling the converters, we can fully understand their behavior. Moreover, this allows an analysis of the state variables and, finally, obtains the voltage gain of the system.

2.1. Cuk Converter

The first step in obtaining the averaged model of a converter is to obtain the equivalent circuit for each switch state. Then, Kirchhoff's laws are used to obtain the equations of the variables of interest. Figure 3 shows the equivalent circuit of the Cuk converter when the MOSFET is on. Equation (1) represents the state-space model of the circuit depicted in Figure 3, where i_1 is the current through the inductor L_1 , v_c is the voltage across the capacitor C , i_2 is the current through the inductor L_2 , v_o is the voltage across the capacitor C_o , L_1 is the inductance value of the inductor L_1 , C is the capacitance value of the capacitor C , L_2 is the inductance value of the inductor L_2 , C_o is the capacitance value of the capacitor C_o , R is the value of the output resistance, and v_{in} is the input voltage.

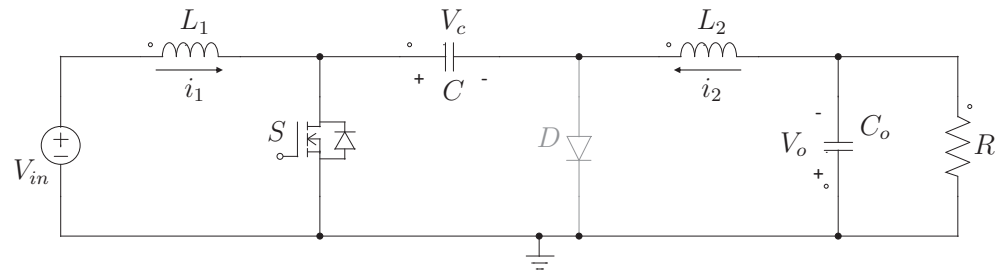


Figure 3. Equivalent circuit of the Cuk converter when the MOSFET is on.

$$\begin{bmatrix} \dot{i}_1 \\ \dot{v}_c \\ \dot{i}_2 \\ \dot{v}_o \end{bmatrix} = \begin{bmatrix} 0 & 0 & 0 & 0 \\ 0 & 0 & -\frac{1}{C} & 0 \\ 0 & \frac{1}{L_2} & 0 & -\frac{1}{L_2} \\ 0 & 0 & \frac{1}{C_o} & -\frac{1}{RC_o} \end{bmatrix} \begin{bmatrix} i_1 \\ v_c \\ i_2 \\ v_o \end{bmatrix} + \begin{bmatrix} \frac{1}{L_1} \\ 0 \\ 0 \\ 0 \end{bmatrix} v_{in} \quad (1)$$

Figure 4 shows the equivalent circuit of the Cuk converter when the MOSFET is off. The state-space model of this circuit is represented in (2).

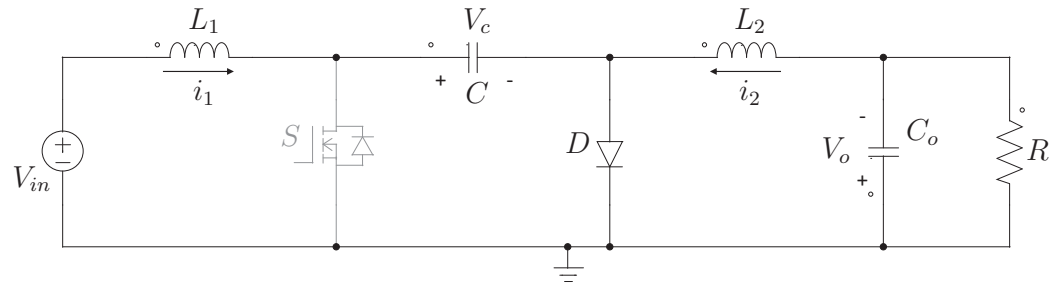


Figure 4. Equivalent circuit of the Cuk converter when the MOSFET is off.

$$\begin{bmatrix} \dot{i}_1 \\ \dot{v}_c \\ \dot{i}_2 \\ \dot{v}_o \end{bmatrix} = \begin{bmatrix} 0 & -\frac{1}{L_1} & 0 & 0 \\ \frac{1}{C} & 0 & 0 & 0 \\ 0 & 0 & 0 & -\frac{1}{L_2} \\ 0 & 0 & \frac{1}{C_o} & -\frac{1}{RC_o} \end{bmatrix} \begin{bmatrix} i_1 \\ v_c \\ i_2 \\ v_o \end{bmatrix} + \begin{bmatrix} \frac{1}{L_1} \\ 0 \\ 0 \\ 0 \end{bmatrix} v_{in} \quad (2)$$

Equations (1) and (2) are used in (3) to obtain the averaged model of the system, where X is the vector of states, A_1 is the matrix that multiplies the vector of states in the model when the MOSFET is on, A_2 is the matrix that multiplies the vector of states in the model when the MOSFET is off, B_1 is the matrix that multiplies the input variable in the model when the MOSFET is on, B_2 is the matrix that multiplies the input variable in the model when the MOSFET is off, d is the duty cycle of the PWM signal applied to the MOSFET, and u is the input variable.

$$\dot{\bar{X}} = [A_1d + A_2(1 - d)]\bar{X} + [B_1d + B_2(1 - d)]\bar{u} \quad (3)$$

Equation (4) shows the state-space averaged model. Finally, this model is linearized. Each variable is replaced by the sum of a large signal and a small signal ($\bar{x} = X + \hat{x}$) to achieve linearization, where \bar{x} is an averaged variable, X is the DC component of the variable, and \hat{x} is the small component of the variable. In this system, the variables are i_1 , i_2 , v_c , v_o , d , and v_{in} .

$$\begin{bmatrix} \dot{\bar{i}}_1 \\ \dot{\bar{v}}_c \\ \dot{\bar{i}}_2 \\ \dot{\bar{v}}_o \end{bmatrix} = \begin{bmatrix} 0 & \frac{\bar{d}-1}{L_1} & 0 & 0 \\ -\frac{\bar{d}-1}{C} & 0 & \frac{\bar{d}}{C} & 0 \\ 0 & \frac{\bar{d}}{L_2} & 0 & -\frac{1}{L_2} \\ 0 & 0 & \frac{1}{C_o} & -\frac{1}{RC_o} \end{bmatrix} \begin{bmatrix} \bar{i}_1 \\ \bar{v}_c \\ \bar{i}_2 \\ \bar{v}_o \end{bmatrix} + \begin{bmatrix} \frac{1}{L_1} \\ 0 \\ 0 \\ 0 \end{bmatrix} \bar{v}_{in} \quad (4)$$

Finally, (5) shows the small-signal model of the Cuk converter. In addition, (6)–(10) show the system’s point of operation that is obtained from computing the DC components of the signal.

$$\begin{bmatrix} \hat{i}_1 \\ \hat{v}_c \\ \hat{i}_2 \\ \hat{v}_o \end{bmatrix} = \begin{bmatrix} 0 & \frac{D-1}{L_1} & 0 & 0 \\ -\frac{D-1}{C} & 0 & \frac{D}{C} & 0 \\ 0 & \frac{D}{L_2} & 0 & -\frac{1}{L_2} \\ 0 & 0 & \frac{1}{C_o} & -\frac{1}{RC_o} \end{bmatrix} \begin{bmatrix} \hat{i}_1 \\ \hat{v}_c \\ \hat{i}_2 \\ \hat{v}_o \end{bmatrix} + \begin{bmatrix} \frac{V_c}{L_1} \\ -\frac{L_1+L_2}{C} \\ \frac{V_c}{L_2} \\ 0 \end{bmatrix} \hat{d} + \begin{bmatrix} \frac{1}{L_1} \\ 0 \\ 0 \\ 0 \end{bmatrix} v_{in} \quad (5)$$

$$\frac{V_c}{V_{in}} = \frac{1}{1-D} \quad (6)$$

$$\frac{V_o}{V_c} = D \quad (7)$$

$$\frac{V_o}{V_{in}} = \frac{D}{1-D} \quad (8)$$

$$\frac{I_2}{I_1} = \frac{1-D}{D} \quad (9)$$

$$I_2 = \frac{V_o}{R} \quad (10)$$

2.2. Sheppard–Taylor Converter

The same methodology was followed to obtain the averaged model of the Sheppard–Taylor converter. Figure 5 shows the equivalent circuit of the converter when the MOSFETs are on. Equation (11) represents the state-space model of this circuit, where i_1 is the current through the inductor L_1 , v_c is the voltage across the capacitor C , i_2 is the current through the inductor L_2 , v_o is the voltage across the capacitor C_o , L_1 is the inductance value of the inductor L_1 , C is the capacitance value of the capacitor C , L_2 is the inductance value of the inductor L_2 , C_o is the capacitance value of the capacitor C_o , R is the value of the output resistance, and v_{in} is the input voltage.

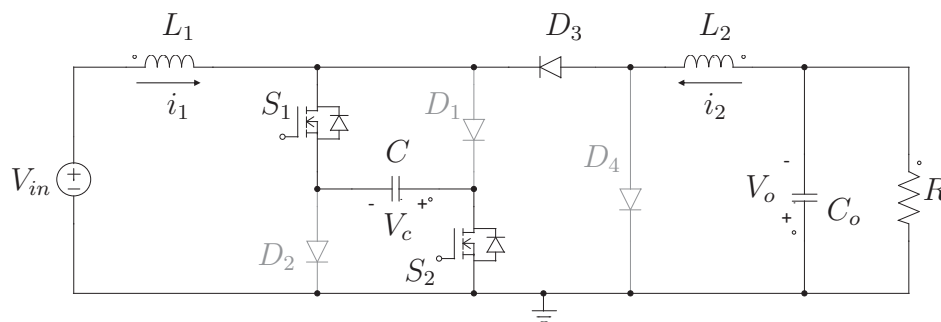


Figure 5. Equivalent circuit of the Sheppard–Taylor converter when the MOSFETs are on.

$$\begin{bmatrix} \dot{i}_1 \\ \dot{v}_c \\ \dot{i}_2 \\ \dot{v}_o \end{bmatrix} = \begin{bmatrix} 0 & \frac{1}{L_1} & 0 & 0 \\ -\frac{1}{C} & 0 & -\frac{1}{C} & 0 \\ 0 & \frac{1}{L_2} & 0 & -\frac{1}{L_2} \\ 0 & 0 & \frac{1}{C_o} & -\frac{1}{RC_o} \end{bmatrix} \begin{bmatrix} i_1 \\ v_c \\ i_2 \\ v_o \end{bmatrix} + \begin{bmatrix} \frac{1}{L_1} \\ 0 \\ 0 \\ 0 \end{bmatrix} v_{in} \quad (11)$$

Figure 6 shows the equivalent circuit of the Sheppard–Taylor converter when the MOSFETs are off. The state-space model of this circuit is represented in (12).

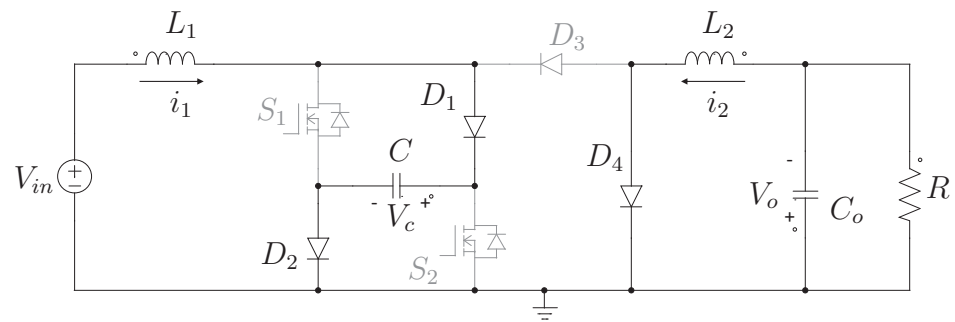


Figure 6. Equivalent circuit of the Sheppard–Taylor converter when the MOSFETs are off.

$$\begin{bmatrix} \dot{i}_1 \\ \dot{v}_c \\ \dot{i}_2 \\ \dot{v}_o \end{bmatrix} = \begin{bmatrix} 0 & -\frac{1}{L_1} & 0 & 0 \\ \frac{1}{C} & 0 & 0 & 0 \\ 0 & 0 & 0 & -\frac{1}{L_2} \\ 0 & 0 & \frac{1}{C_o} & -\frac{1}{RC_o} \end{bmatrix} \begin{bmatrix} i_1 \\ v_c \\ i_2 \\ v_o \end{bmatrix} + \begin{bmatrix} \frac{1}{L_1} \\ 0 \\ 0 \\ 0 \end{bmatrix} v_{in} \tag{12}$$

Equation (13) shows the state-space averaged model of the Sheppard–Taylor converter.

$$\begin{bmatrix} \dot{\bar{i}}_1 \\ \dot{\bar{v}}_c \\ \dot{\bar{i}}_2 \\ \dot{\bar{v}}_o \end{bmatrix} = \begin{bmatrix} 0 & \frac{2\bar{d}-1}{L_1} & 0 & 0 \\ -\frac{2\bar{d}-1}{C} & 0 & -\frac{\bar{d}}{C} & 0 \\ 0 & \frac{\bar{d}}{L_2} & 0 & -\frac{1}{L_2} \\ 0 & 0 & \frac{1}{C_o} & -\frac{1}{RC_o} \end{bmatrix} \begin{bmatrix} \bar{i}_1 \\ \bar{v}_c \\ \bar{i}_2 \\ \bar{v}_o \end{bmatrix} + \begin{bmatrix} \frac{1}{L_1} \\ 0 \\ 0 \\ 0 \end{bmatrix} \bar{v}_{in} \tag{13}$$

Finally, (14) shows the small-signal model of this converter. Furthermore, (15)–(19) show the point of operation of the system.

$$\begin{bmatrix} \hat{i}_1 \\ \hat{v}_c \\ \hat{i}_2 \\ \hat{v}_o \end{bmatrix} = \begin{bmatrix} 0 & \frac{2D-1}{L_1} & 0 & 0 \\ -\frac{2D-1}{C} & 0 & -\frac{D}{C} & 0 \\ 0 & \frac{D}{L_2} & 0 & -\frac{1}{L_2} \\ 0 & 0 & \frac{1}{C_o} & -\frac{1}{RC_o} \end{bmatrix} \begin{bmatrix} \hat{i}_1 \\ \hat{v}_c \\ \hat{i}_2 \\ \hat{v}_o + \frac{2V_c}{L_1} \\ -\frac{2I_1 + I_2}{C} \\ \frac{V_c}{L_2} \\ 0 \end{bmatrix} \hat{d} + \begin{bmatrix} \frac{1}{L_1} \\ 0 \\ 0 \\ 0 \end{bmatrix} \hat{v}_{in} \tag{14}$$

$$\frac{V_c}{V_{in}} = \frac{1}{1 - 2D} \tag{15}$$

$$\frac{V_o}{V_c} = D \tag{16}$$

$$\frac{V_o}{V_{in}} = \frac{D}{1 - 2D} \tag{17}$$

$$\frac{I_2}{I_1} = \frac{1 - 2D}{D} \tag{18}$$

$$I_2 = \frac{V_o}{R} \tag{19}$$

Analyzing (5) and (14), it can be seen that the model is very similar for both converters. Both are fourth-order systems as they have four storage devices. Furthermore, the matrices paired with the state vector and the input variables are very similar. The terms with value 0 are the same for each model. Therefore, the complexity of designing a controller is similar in each converter, and the behavior will be alike.

3. Simulation Results

In this section, we present the simulations that were performed for both converters. The software PSIM was used to carry out these simulations because it has been specifically developed for power electronics applications. These simulations reveal the behavior of each converter. In addition, it becomes possible to demonstrate the operating point and the gain obtained through the averaged model. Finally, the stress on the switches is shown. The value of the elements is the same in both converters, because they present the same distribution of storage devices. Table 2 shows the value of the components used in both converters. In addition, the converters are operated to obtain an output voltage of 5 V.

Table 2. Value of the components used in the simulation.

Component	Symbol	Value
Input Voltage	V_{in}	10 V
Inductor 1	L_1	210 μ H
Capacitor	C	10 μ F
Inductor 2	L_2	735 μ H
Output Capacitor	C_o	1 mF
Load	R	10 Ω

3.1. Cuk Converter

The first step is to compute the duty cycle needed to guarantee the desired output voltage. According to (8), a 0.33 duty cycle was imposed on the PWM signal of the switches. Figure 7 shows the voltage present in the storage elements of the Cuk converter. It can be appreciated that the output voltage reaches a steady state at 5 V. Furthermore, the voltage across the capacitor C is stabilized at 15 V. Finally, it can be seen that the system reaches a steady state within 10 ms.

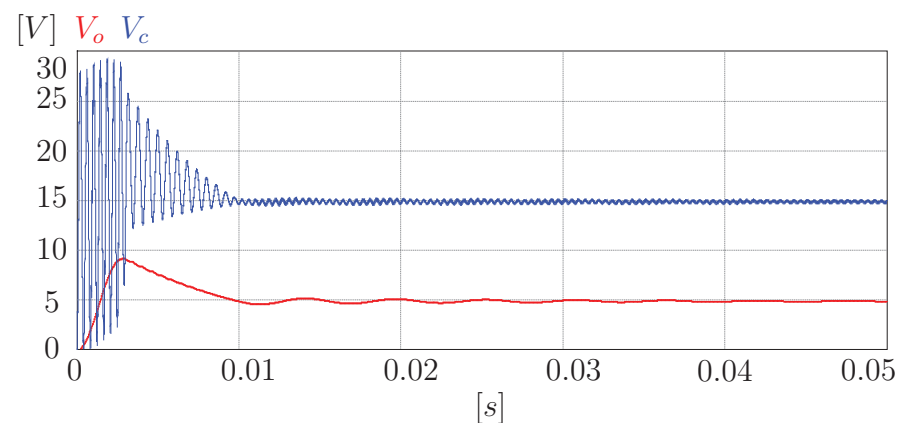


Figure 7. Voltage of the capacitors present in the Cuk converter.

Figure 8 shows the currents in both inductors for this topology. It can be seen that they are transient where the currents i_1 and i_2 reach almost 6 A. However, in less than 5 ms, the current is under 1 A. Moreover, the average steady-state value is 0.5 A for i_2 and 0.25 A for i_1 . These values correspond to those obtained from (10) and (9). Finally, current i_1 has a greater ripple than current i_2 because the value of inductance L_1 is lower than the value of inductance L_2 .

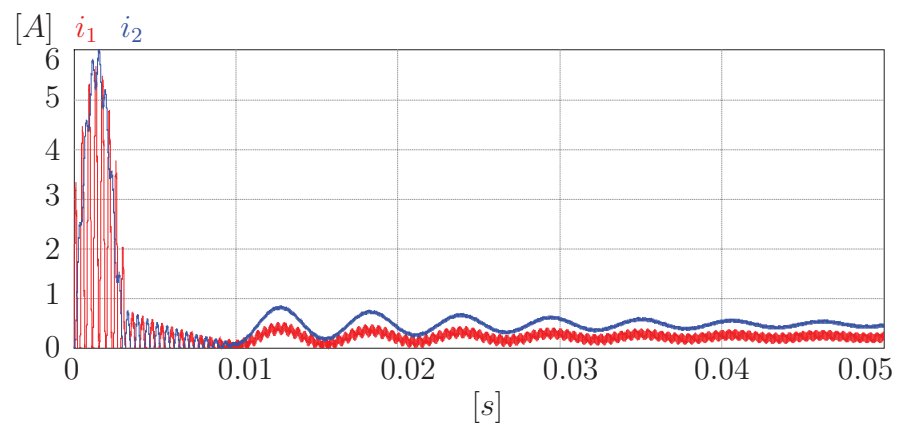


Figure 8. Current of the inductors present in the Cuk converter.

In addition, simulations were performed to analyze the stress of the switches in this architecture. Figure 9 shows the voltage stress on the MOSFET. It can be seen that the voltage that this element must withstand is the voltage presented by the capacitor C . Although not illustrated in this work, it was verified that the diode must also withstand the voltage of the capacitor C . We do not show this graph because it is the same as Figure 9. However, when zoomed in, it is possible to see that the voltage appears on the diode when the PWM signal is high, while it appears on the MOSFET when the PWM signal is low, as shown in Figure 10. Finally, the current stress suffered by the switches was checked. Both switches must withstand the sum of the currents i_1 and i_2 .

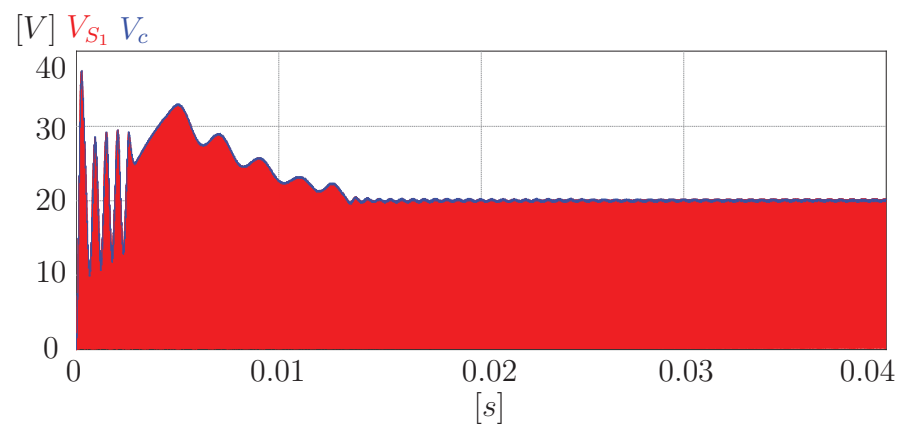


Figure 9. Voltage stress in the switch S_1 of the Sheppard–Taylor converter.

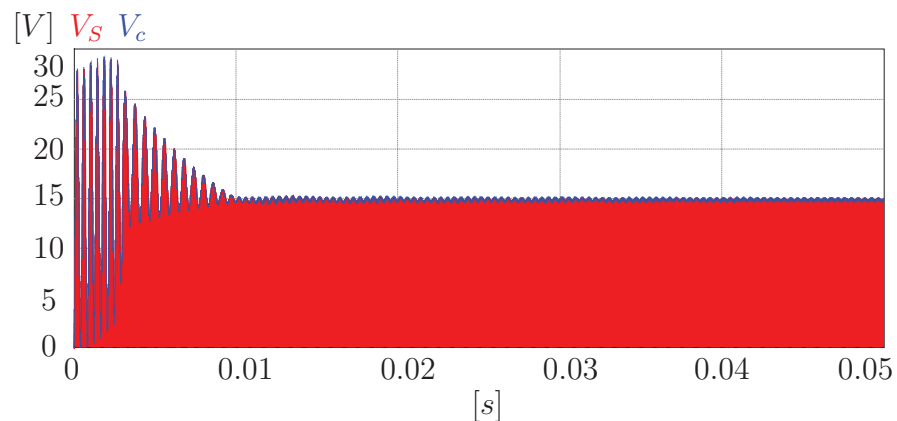


Figure 10. Voltage stress in the switch S of the Cuk converter.

3.2. Sheppard–Taylor Converter

In this simulation, a 0.25 duty cycle was imposed on the PWM signal of the MOSFETs. In this way, the desired output voltage of 5 V was guaranteed, as can be seen in (17). Figure 11 shows the voltages obtained in the simulation of the Sheppard–Taylor converter. It can be seen that the desired output voltage was reached. Furthermore, the voltage across the capacitor C is stabilized at 20 V. Finally, it can be seen that the system reaches a steady state within 15 ms.

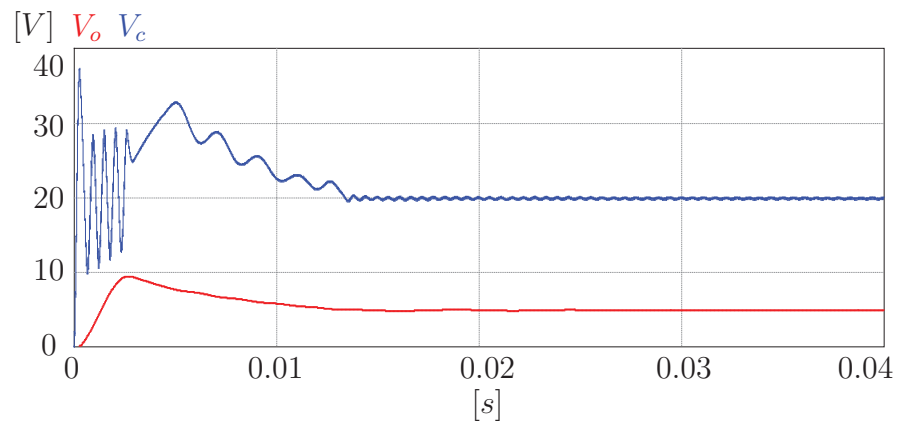


Figure 11. Voltage of the capacitors present in the Sheppard–Taylor converter.

Figure 12 shows the currents in both inductors. It can be seen that they are transient where the currents i_1 and i_2 exceed 4 and 6 A, respectively. However, they stabilize within 5 ms. Moreover, the average steady-state value is 0.5 A for i_2 and 0.25 A for i_1 . These values verify the operating point obtained from (19) and (18). Finally, current i_1 has a greater ripple than current i_2 , for the same reason that $L_2 > L_1$ in the Cuk converter.

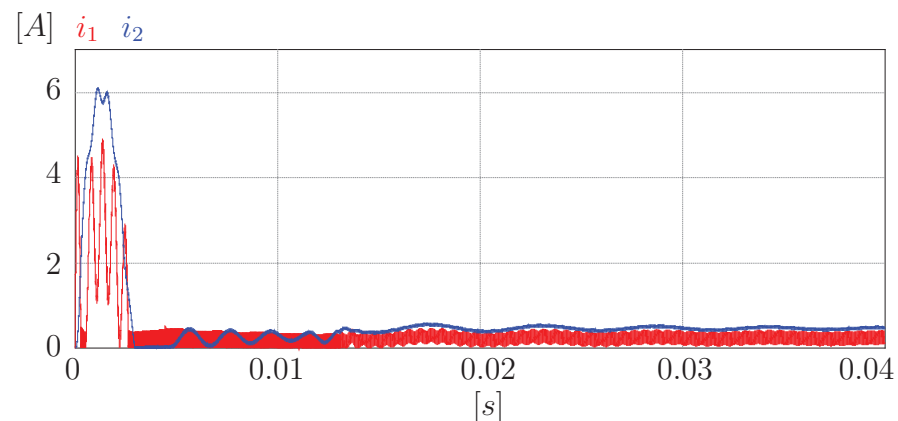


Figure 12. Current of the inductors present in the Sheppard–Taylor converter.

Finally, Figure 9 shows the voltage stress on MOSFET S_1 . It can be seen that the voltage that this element must withstand is the voltage presented by the capacitor C . After conducting several experiments with all the switches, it was concluded that the voltage stress of these elements is the voltage of the capacitor C . However, the voltage appears in the elements in different states of the PWM signal. When the PWM signal is high, the voltage V_c appears on the diodes D_1 , D_2 , and D_4 , while when the signal is low, the voltage appears on the elements S_1 , S_2 , and D_3 . Current stress-wise, it was concluded that diodes D_1 and D_2 must withstand current i_1 , diodes D_3 and D_4 must withstand current i_2 , and the MOSFETs must withstand the sum of i_1 and i_2 . This behavior can be verified by analyzing Figures 5 and 6, taking into account the specific test conditions.

In this section, verifying the previously obtained operating point is possible. Furthermore, it was evidenced that the voltage of capacitor C determines the stress of the switches. However, it could be seen that the voltage V_c in the Cuk converter is lower than in the Sheppard–Taylor converter. Therefore, the voltage stress on the switches will be lower in the Cuk converter. Once again, the Cuk converter presents the most desirable feature. In addition, the current of both inductors in the steady state was the same in both converters. Although the comparison based on the simulation results has been helpful, it is essential to note that this is only a point of operation. Can these conclusions be extended to the entire operating region of the converters? This question and others will be answered in the next section.

4. Discussion

So far, we have analyzed different parameters and considered them in comparing both converters. In all cases, the Cuk converter presented the most desirable features. Table 3 summarizes the main results according to the voltage and current of both methods.

Table 3. Principal results obtained in the simulation.

Variable	Cuk Converter	Sheppard–Taylor Converter
Stabilized voltage in capacitor (V)	10	20
Steady time (ms)	10	15
Average steady state for I_1 (A)	0.5	0.25
Average steady state for I_2 (A)	0.5	0.25
Reaching current I_1 (A)	6	6
Reaching current I_1 (A)	4	6

Moreover, the most critical state was considered when performing the simulations and obtaining the results. In this section, we will conduct an in-depth study of both converters. In this way, we can determine if the Sheppard–Taylor converter is underrated and whether it may be the better converter in some applications.

The Cuk converter features fewer switches and only has one MOSFET and one diode, while the Sheppard–Taylor converter features two MOSFETs and four diodes. Therefore, there is less initial investment in the Cuk converter. In addition, this causes it to have fewer power losses, because the current passes through more elements in the Sheppard–Taylor converter, resulting in more significant losses in conduction and switching power.

As stated before, both converters have a similar structure when analyzing the linearized model. Therefore, the complexity of designing the controller will be similar for both converters. However, differences can be seen at the point of operation. Figure 13 shows the voltage gain as a function of D , given (8) and (17). It can be seen that the Cuk converter achieves a higher gain. However, both converters have the possibility, in theory, of having infinite gain. In practice, getting so close to this critical point is impossible. The Cuk converter can achieve a higher gain because it has a smoother curve. It should also be noted that the $[0.5–1]$ duty cycle region in the Sheppard–Taylor converter cannot be used. If a duty cycle of this region is used, it will cause the polarity of the voltages to change, leading to a short circuit. Finally, it can be concluded that both converters can reduce or boost the input voltage. The Cuk converter must operate with a duty cycle of less than 0.5 to reduce the input voltage and with a duty cycle greater than 0.5 to raise it. The Sheppard–Taylor converter must operate with a duty cycle of less than 0.33 to reduce the input voltage, while the duty cycle must be greater than 0.33 and less than 0.5 to boost it.

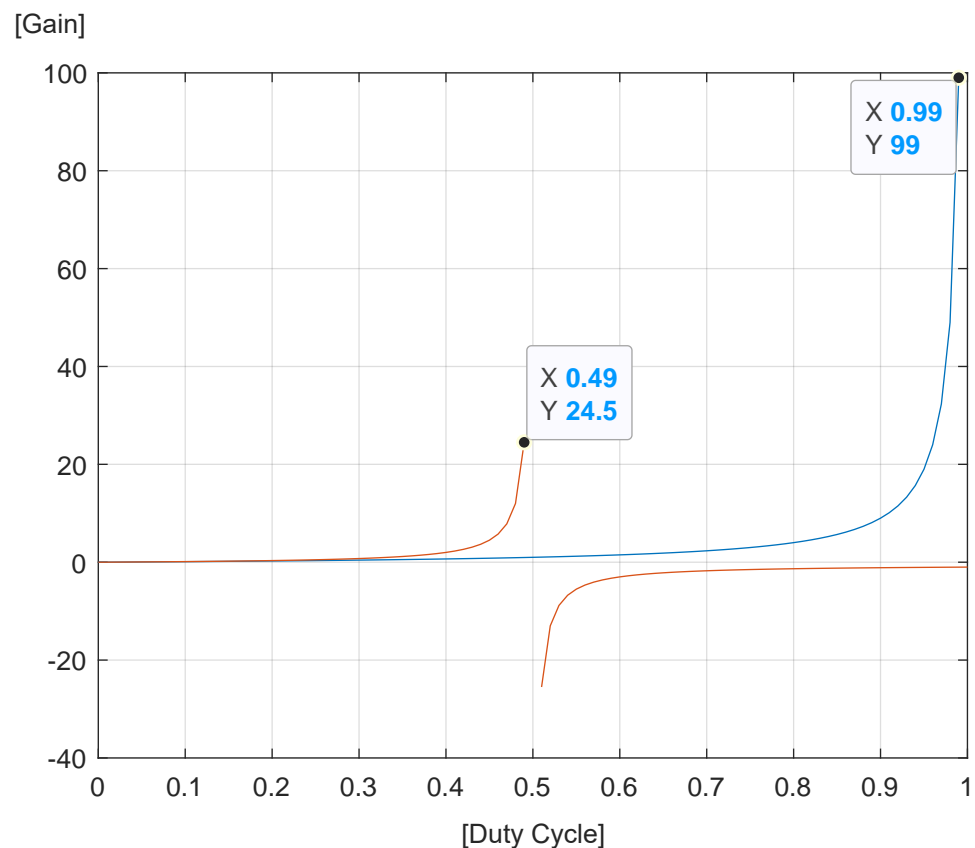


Figure 13. Voltage gain of both converters for all possible duty cycles, where the blue line represents the Cuk converter and the red line represents the Sheppard–Taylor converter.

The stress analysis in the switches presented in the previous section was carried out from a narrow perspective because only one operating point was analyzed. Therefore, it cannot be generalized to the entire operating region. However, it can be generalized that this stress depends on the voltage of the intermediate capacitor (V_c). By substituting (7) into (6), we obtain (20), which represents the operating point of the voltage V_c in the Cuk converter. Performing this procedure for the Sheppard–Taylor converter with (15) and (16) yields (21). Analyzing (20) and (21), it can be concluded that the Cuk converter switches will always present lower voltage stress.

$$V_c = V_{in} + V_o \quad (20)$$

$$V_c = V_{in} + 2V_o \quad (21)$$

The same analysis can be carried out to obtain the current stress, obtaining $I_2 V_o = I_1 V_{in}$. This result was expected, because the output power is ideally equal to the input power. In an application, we have fixed values for the input voltage, output voltage, and current I_2 (determined by the load). Therefore, the current I_1 should be the same for both converters. However, as the Sheppard–Taylor converter has greater power losses, the converter will need to be stressed a bit more to guarantee the power output.

Finally, the sizing of the storage devices was analyzed. This sizing is performed with (1) and (11). For example, the equation of the derivative of i_1 that is obtained from (1) is

$$\frac{di_1}{dt} = \frac{V_{in}}{L_1}$$

Equation (22) represents the minimum value required for L_1 in the Cuk converter, where Δt is the time the MOSFET will be on, and Δi_1 is the allowed current ripple. Substituting Δt for DT , where T is the period of the PWM signal, and using Equations (7) and (20) yields (23). If the same procedure is carried out for the Sheppard–Taylor converter, (24) is obtained. Furthermore, the same analysis was carried out for the elements L_2 and C . The study of the capacitor C_o yields the same equation for both converters. Therefore, the size of this element to guarantee the desired conditions will be the same for both converters.

$$L_1 = \frac{\Delta t V_{in}}{\Delta i_1} \quad (22)$$

$$L_{1min_Cuk} = \frac{V_{in} V_o}{V_{in} + V_o} \frac{T}{\Delta i_1} \quad (23)$$

$$L_{1min_ST} = \frac{2(V_{in} + V_o) V_o}{V_{in} + 2V_o} \frac{T}{\Delta i_1} \quad (24)$$

Equation (25) represents the minimum value of L_2 for the Cuk converter, while (26) is obtained for the Sheppard–Taylor converter. Finally, (27) represents the minimum value of the capacitor C for the Cuk converter, while (28) represents the minimum value of this capacitor for the Sheppard–Taylor converter. Analyzing these equations, it can be concluded that there is a constant that can depend on the period of the PWM signal, the ripple allowed for a variable, and the load for both converters. This constant is multiplied by a factor that depends on the input and output voltage. A larger factor is less desirable, because it indicates that a larger storage device will be needed to meet the design requirements.

$$L_{2min_Cuk} = \frac{V_{in} V_o}{V_{in} + V_o} \frac{T}{\Delta i_2} \quad (25)$$

$$L_{2min_ST} = \frac{(V_{in} + V_o) V_o}{V_{in} + 2V_o} \frac{T}{\Delta i_2} \quad (26)$$

$$C_{min_Cuk} = \frac{V_o^2}{V_{in} + V_o} \frac{T}{R \Delta V_c} \quad (27)$$

$$C_{min_ST} = \frac{(V_{in} + V_o) V_o^2}{V_{in} (V_{in} + 2V_o)} \frac{T}{R \Delta V_c} \quad (28)$$

The above equations can be used to obtain the minimum value of the storage elements in each converter and should be of the lowest possible value for devices. For each component, we take the switching period, the ripple allowed in the variable of interest, and the resistance as fixed values. In this way, the minimum value of each element depends on the input and output voltage desired in the application. We use MATLAB to obtain the value of this factor in each equation. Subsequently, we graph it in a single figure to show which factor is larger. The larger factor will cause a larger inductance or capacitance and, therefore, indicate a more expensive item. The input voltage was taken from 10 to 400 V to verify a large spectrum of applications. Moreover, for each input, an output in the region $[V_{in}/3; 3V_{in}]$ was analyzed. Figure 14 shows the graphs of these factors for each of the studied storage devices. In all cases, the surface associated with the Sheppard–Taylor converter is above the surface of the Cuk converter. Therefore, to keep a variable of interest within an allowed ripple, the Sheppard–Taylor converter requires larger storage elements than the Cuk converter.

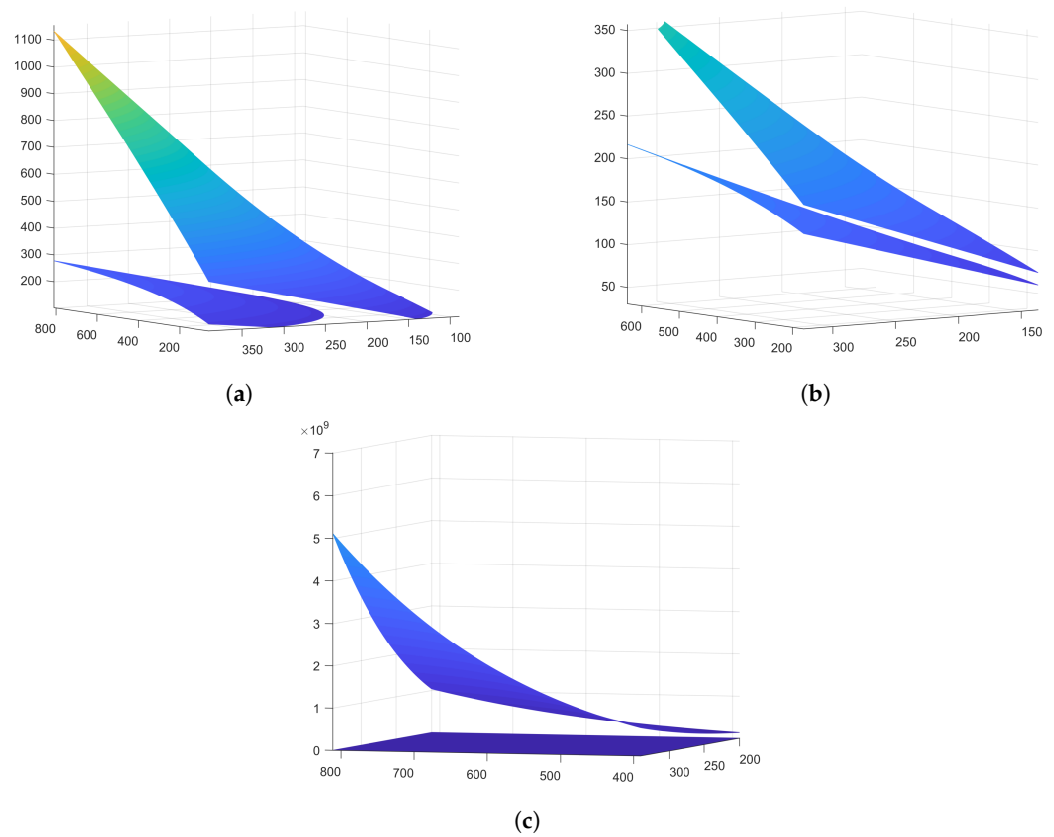


Figure 14. Factors associated with storage devices: (a) L_1 , (b) L_2 , and (c) C.

These graphs also show that the storage elements of the Sheppard–Taylor converter are more stressed. For example, the inductor L_1 must be larger because the voltage V_L is greater. Nevertheless, this can also be perceived as an advantage. Figure 15 shows the energy extracted from the source using the data from Table 2. It can be seen that, for storage elements of the same dimension, the Sheppard–Taylor converter transfers more energy. Therefore, the advantage of the Sheppard–Taylor converter over the Cuk converter is shown in this behavior. We believe that the only applications that justify using a Sheppard–Taylor converter are those where a high energy transfer rate is required. Some applications that present this challenge are chargers for electric vehicles, motor drivers, and cell equalizers.

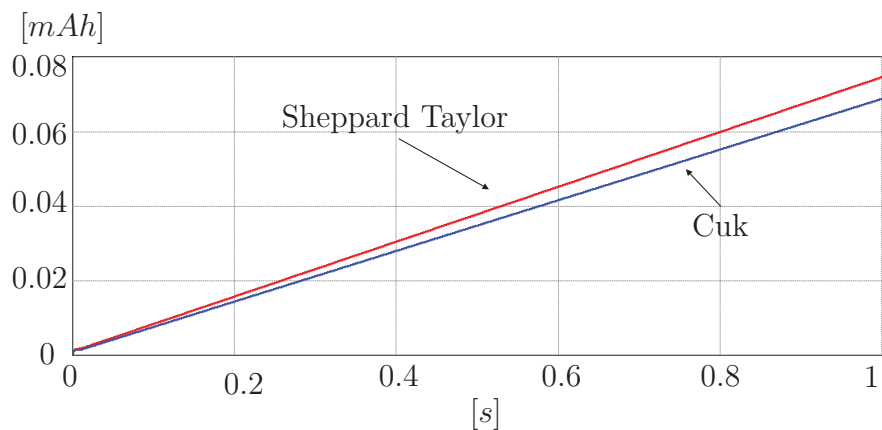


Figure 15. Voltage of the capacitors present in the Cuk converter.

Equation (29) shows the conduction losses in the Sheppard–Taylor converter. If it is assumed that the diodes, the MOSFETs, and the inductors present the same resistance, the

Equation (30) is obtained. On the other hand, the Equation (31) shows the conduction losses in the Cuk converter. In all the elements of the sum, except the one that represents the losses due to the current i_2 when the MOSFETs are off, the Sheppard–Taylor equation presents more elements. This behavior was expected because the Sheppard–Taylor converter has more elements. Therefore, this will imply higher conduction losses in the Sheppard–Taylor converter. Another component of total losses is switching losses. Equation (32) represents the switching losses in the Sheppard–Taylor converter. On the other hand, Equation (33) represents the switching losses in the Cuk converter. It can be seen that the losses in the Sheppard–Taylor converter are twice greater than the losses obtained in the Cuk. This is because it features one more MOSFET, and the stress on these elements is the same for both converters.

$$P_{L_Cond} = i_1^2(D(R_{on_V_{in}} + R_{L_1} + R_{on_S_1} + R_{on_S_2} + R_C) + (1 - D)(R_{on_V_{in}} + R_{L_1} + R_{on_D_1} + R_{on_D_2} + R_C) + i_2^2(D(R_{on_C_O} + R_{L_2} + R_{on_S_1} + R_{on_S_2} + R_C + R_{on_D_3}) + (1 - D)(R_{on_C_O} + R_{L_2} + R_{on_D_4})) \quad (29)$$

$$P_{L_Cond} = i_1^2(D(R_{on_V_{in}} + R_L + 2R_{on_S} + R_C) + (1 - D)(R_{on_V_{in}} + R_L + 2R_{on_D} + R_C) + i_2^2(D(R_{on_C_O} + R_L + 2R_{on_S} + R_C + R_{on_D}) + (1 - D)(R_{on_C_O} + R_L + R_{on_D})) \quad (30)$$

$$P_{L_Cond} = i_1^2(D(R_{on_V_{in}} + R_{L_1} + R_{on_S}) + (1 - D)(R_{on_V_{in}} + R_L + R_C + R_{on_D}) + i_2^2(D(R_{on_C_O} + R_{L_2} + R_C + R_{on_S}) + (1 - D)(R_{on_C_O} + R_{L_2} + R_{on_D})) \quad (31)$$

$$P_{L_Sw} = 2V_C(i_1 + i_2)f_{sw}(t_r + t_f) \quad (32)$$

$$P_{L_Sw} = V_C(i_1 + i_2)f_{sw}(t_r + t_f) \quad (33)$$

Cuk converters offer high energy efficiency, minimizing power losses during battery charging and discharging processes, and thus maximizing the overall efficiency of the BMS. This is crucial for optimizing the range and performance of electric vehicles. Moreover, these converters can handle a wide range of input voltages, making them suitable for various battery chemistries and charging scenarios. They provide flexibility in adapting to different battery configurations, ensuring compatibility with diverse electric vehicle platforms. However, they have a more complex control scheme compared to other converter topologies. They require additional components and control algorithms, which can increase the complexity and cost of the BMS implementation. Finally, Cuk converters may result in higher manufacturing and maintenance costs for the BMS. The additional components and control requirements can add to the overall system cost, making it less economically feasible for certain applications.

As future work, this method can be performed in a real scenario in order to analyze in detail the modeling of the current and voltage derivative. This would allow to obtain the value of the capacitor to be precisely determined to ensure a desired level of ripple in the current or voltage.

Sheppard–Taylor converters offer a simple control scheme and require fewer components compared to more complex converter topologies. This simplicity makes them easier to implement and maintain, and they tend to be more cost-effective. Furthermore, Sheppard–Taylor converters provide good load regulation and a fast transient response, ensuring stable power delivery to electric vehicle systems. In addition, because this circuit

is capable of processing small voltage inputs [36], a Sheppard–Taylor configuration is possible in applications where systems require low voltage, such as the last-mile cargo distribution [37]. This is important for maintaining consistent performance and protecting the battery and other electronic components. Nevertheless, these converters typically function as step-down, limiting their application in scenarios where step-up voltage conversion is required. They may not be suitable for certain battery charging or power delivery requirements, restricting their versatility in some electric vehicle applications.

5. Conclusions

In this study, a comprehensive comparison was conducted between the Cuk and Sheppard–Taylor converters for their application in Battery Management Systems (BMS) of electric vehicles. Various parameters, including the number of components, model complexity, and stress on parts, were carefully evaluated. The findings revealed that both converters exhibited similar behaviors and presented models of the same complexity. Additionally, it was determined that both converters require a similar level of difficulty in controller design.

Based on the analysis, the Cuk converter demonstrated notable advantages, such as high efficiency and a wide input voltage range. These characteristics contribute to maximizing the overall efficiency and performance of electric vehicles. However, it should be noted that the implementation of the Cuk converter may involve a potential cost increase due to its complex control scheme and additional components.

On the other hand, the Sheppard–Taylor converter offers distinct advantages, including low cost and good load regulation. Its simplicity in terms of the control scheme and fewer components make it an attractive option for BMS implementation, especially for cost-sensitive applications. Nevertheless, it is important to consider the limited voltage conversion capability of the Sheppard–Taylor converter, as it may not be suitable for certain charging or power delivery requirements in electric vehicles.

Ultimately, the choice between the Cuk and Sheppard–Taylor converters depends on the specific requirements and trade-offs that need to be considered. Factors such as efficiency, complexity, cost, and compatibility with the electric vehicle's BMS should be thoroughly assessed to make an informed decision. This study provides valuable insights into the strengths and limitations of each converter, aiding researchers and practitioners in selecting the most suitable converter for their electric vehicle applications.

Author Contributions: Conceptualization, A.A.-D. and J.R.-R.; Methodology, R.V.C.-S. and J.R.-R.; Software, A.A.-D.; Validation, A.A.-D. and R.V.C.-S.; Formal Analysis, J.R.-R., A.A.E.-B. and J.M.Á.-A.; Investigation, A.A.-D.; Resources, J.R.-R. and R.V.C.-S.; Data Curation, A.A.-D. and J.R.-R.; Writing—Original Draft Preparation, Review, and Editing, A.A.-D., J.R.-R., R.V.C.-S., A.A.E.-B. and J.M.Á.-A. All authors have read and agreed to the published version of the manuscript.

Funding: This research was funded by the National Council on Science and Technology and FOPER under grant FIN02455.

Data Availability Statement: Not applicable.

Conflicts of Interest: The authors declare no conflict of interest.

References

1. Estévez-Bén, A.A.; Alvarez-Diazcomas, A.; Rodríguez-Reséndiz, J. Transformerless multilevel voltage-source inverter topology comparative study for PV systems. *Energies* **2020**, *13*, 3261. [[CrossRef](#)]
2. Tzermias, G.; Akehurst, S.; Burke, R.; Brace, C.; George, S.; Bernards, J.; Smith, C. Methodology for the Optimisation of Battery Hybrid Energy Storage Systems for Mass and Volume Using a Power-To-Energy Ratio Analysis. *Batteries* **2021**, *7*, 37. [[CrossRef](#)]
3. Kusch-Brandt, S. Urban Renewable Energy on the Upswing: A Spotlight on Renewable Energy in Cities in REN21's "Renewables 2019 Global Status Report". *Resources* **2019**, *8*, 139. [[CrossRef](#)]
4. Wang, Y.; Li, W.; Liu, Z.; Li, L. An Energy Management Strategy for Hybrid Energy Storage System Based on Reinforcement Learning. *World Electr. Veh. J.* **2023**, *14*, 57. [[CrossRef](#)]

5. Alvarez-Diazcomas, A.; López, H.; Carrillo-Serrano, R.V.; Rodríguez-Reséndiz, J.; Vázquez, N.; Herrera-Ruiz, G. A novel integrated topology to interface electric vehicles and renewable energies with the grid. *Energies* **2019**, *12*, 4091. [[CrossRef](#)]
6. Bhajana, V.V.S.K.; Drabek, P.; Jara, M.; Peroutka, Z. Comparison of main design concepts of auxiliary drives for DC catenary fed light traction vehicles: SiC JFET vs. Si IGBT technology. *EPE J.* **2020**, *31*, 17–31. [[CrossRef](#)]
7. Lee, H.; Smet, V.; Tummala, R. A review of SiC power module packaging technologies: Challenges, advances, and emerging issues. *IEEE J. Emerg. Sel. Top. Power Electron.* **2019**, *8*, 239–255. [[CrossRef](#)]
8. Rashid, M.H. *Power Electronics Handbook*; Butterworth-Heinemann: Oxford, UK, 2017.
9. Hidalgo, H.; Vázquez, N.; Orosco, R.; Huerta-Ávila, H.; Pinto, S.; Estrada, L. Floating Interleaved Boost Converter with Zero-Ripple Input Current Using Variable Inductor. *Technologies* **2023**, *11*, 21. [[CrossRef](#)]
10. Koundi, M.; El Idrissi, Z.; El Fadil, H.; Belhaj, F.Z.; Lassoui, A.; Gaouzi, K.; Rachid, A.; Giri, F. State-Feedback Control of Interleaved Buck–Boost DC–DC Power Converter with Continuous Input Current for Fuel Cell Energy Sources: Theoretical Design and Experimental Validation. *World Electr. Veh. J.* **2022**, *13*, 124. [[CrossRef](#)]
11. Cuk, S.; Middlebrook, R. A new optimum topology switching dc-to-dc converter. In Proceedings of the 1977 IEEE Power Electronics Specialists Conference, Palo Alto, CA, USA, 14–16 June 1977; IEEE: Piscataway, NJ, USA, 1977; pp. 160–179.
12. Zhang, Z.; Cuk, S. A high efficiency 500 W step-up Cuk converter. In Proceedings of the Proceedings IPEMC 2000—Third International Power Electronics and Motion Control Conference (IEEE Cat. No. 00EX435), Beijing, China, 15–18 August 2000; IEEE: Piscataway, NJ, USA, 2000; Volume 2, pp. 909–914.
13. Durán, E.; Galán, J.; Andújar, J.; Sidrach-de Cardona, M. A new method to obtain IV characteristics curves of photovoltaic modules based on SEPIC and cuk converters. *EPE J.* **2008**, *18*, 5–15. [[CrossRef](#)]
14. Cocor, A.; Florescu, A.; Popescu, A.M.; Stoichescu, D.A.; Oprea, S. Power supply blocks with Cúk and self-lift Cúk converters for telecommunication sites. In Proceedings of the 2014 International Symposium on Fundamentals of Electrical Engineering (ISFEE), Bucharest, Romania, 28–29 November 2014; IEEE: Piscataway, NJ, USA, 2014; pp. 1–6.
15. Maroti, P.K.; Padmanaban, S.; Wheeler, P.; Blaabjerg, F.; Rivera, M. Modified high voltage conversion inverting cuk DC-DC converter for renewable energy application. In Proceedings of the 2017 IEEE Southern Power Electronics Conference (SPEC), Puerto Varas, Chile, 4–7 December 2017; IEEE: Piscataway, NJ, USA, 2017; pp. 1–5.
16. Kumar, K.; Babu, N.R.; Prabhu, K. Analysis of integrated Boost-Cuk high voltage gain DC-DC converter with RBFN MPPT for solar PV application. In Proceedings of the 2017 Innovations in Power and Advanced Computing Technologies (i-PACT), Vellore, India, 21–22 April 2017; IEEE: Piscataway, NJ, USA, 2017; pp. 1–6.
17. Pandey, R.; Singh, B. A power-factor-corrected LLC resonant converter for electric vehicle charger using Cuk converter. *IEEE Trans. Ind. Appl.* **2019**, *55*, 6278–6286. [[CrossRef](#)]
18. Pathare, P.S.; Panchade, V. Power quality improvement of BLDC motor drive using Cuk PFC converter. In Proceedings of the 2020 IEEE International Conference on Computing, Power and Communication Technologies (GUCON), Greater Noida, India, 2–4 October 2020; IEEE: Piscataway, NJ, USA, 2020; pp. 177–181.
19. Sheppard, D.; Taylor, B. A new converter topology imparts non-pulsating currents to input and output lines. *Proc. PCI/Motor-Con* **1983**, *60*–73.
20. Bist, V.; Singh, B. A PFC based bridgeless Sheppard-Taylor converter fed brushless DC motor drive. In Proceedings of the 2014 Innovative Applications of Computational Intelligence on Power, Energy and Controls with Their Impact on Humanity (CIPECH), Ghaziabad, India, 28–29 November 2014; IEEE: Piscataway, NJ, USA, 2014; pp. 262–267.
21. Singh, P.; Vinjamuri, R.; Wang, X.; Reisner, D. Design and implementation of a fuzzy logic-based state-of-charge meter for Li-ion batteries used in portable defibrillators. *J. Power Sources* **2006**, *162*, 829–836. [[CrossRef](#)]
22. Kushwaha, R.; Singh, B. An EV battery charger based on PFC Sheppard Taylor Converter. In Proceedings of the 2016 National Power Systems Conference (NPSC), Bhubaneswar, India, 19–21 December 2016; IEEE: Piscataway, NJ, USA, 2016; pp. 1–6.
23. Abedi, M.; Ernzen, B. A hybrid-switching based bridgeless PFC converter for on-board battery chargers using predictive current control. *Int. J. Renew. Energy Res. (IJRER)* **2012**, *2*, 645–651.
24. Tse, C.K.; Chow, M. Single stage high power factor converter using the Sheppard-Taylor topology. In Proceedings of the PESC Record. 27th Annual IEEE Power Electronics Specialists Conference, Baveno, Italy, 23–27 June 1996; IEEE: Piscataway, NJ, USA, 1996; Volume 2, pp. 1191–1197.
25. Soediby; Amri, B.; Ashari, M. The comparative study of Buck-boost, Cuk, Sepic and Zeta converters for maximum power point tracking photovoltaic using P&O method. In Proceedings of the 2015 2nd International Conference on Information Technology, Computer, and Electrical Engineering (ICITACEE), Semarang, Indonesia, 16–18 October 2015; IEEE: Piscataway, NJ, USA, 2015; pp. 327–332.
26. Sakasegawa, E.; Chishiki, R.; Sedutsu, R.; Soeda, T.; Haga, H.; Kennel, R.M. Comparison of Interleaved Boost Converter and Two-Phase Boost Converter Characteristics for Three-Level Inverters. *World Electr. Veh. J.* **2023**, *14*, 7. [[CrossRef](#)]
27. Raghavendra, K.V.G.; Zeb, K.; Muthusamy, A.; Krishna, T.; Kumar, S.; Kim, D.H.; Kim, M.S.; Cho, H.G.; Kim, H.J. A comprehensive review of DC–DC converter topologies and modulation strategies with recent advances in solar photovoltaic systems. *Electronics* **2020**, *9*, 31. [[CrossRef](#)]
28. Kanaan, H.Y.; Al-Haddad, K. A unified approach for the analysis of single-phase power factor correction converters. In Proceedings of the IECON 2011—37th Annual Conference of the IEEE Industrial Electronics Society, Melbourne, VIC, Australia, 7–10 November 2011; IEEE: Piscataway, NJ, USA, 2011; pp. 1167–1172.

29. Mondal, S.; Nandi, A.; Mallick, I.; Ghosh, C.; Giri, A. Performance evaluation of brushless DC motor drive for three different types of MOSFET based DC-DC converters. In Proceedings of the 2017 Devices for Integrated Circuit (DevIC), Kalyani, India, 23–24 March 2017; IEEE: Piscataway, NJ, USA, 2017; pp. 589–593.
30. Shen, Y.; Xia, J.; Cai, C. Flicker-Free LED Driver Based on Cuk Converter with Integrated Magnetics. *World Electr. Veh. J.* **2023**, *14*. [[CrossRef](#)]
31. Xie, W.; Luo, W.; Qin, Y. Integrated DC/DC Converter Topology Study for Fuel Cell Hybrid Vehicles with Two Energy Sources. *World Electr. Veh. J.* **2023**, *14*, 9. [[CrossRef](#)]
32. Wang, X.; Tan, Z.; Cai, L.; Lei, G.; Dai, N. Bi-Directional Cuk Equalizer-Based Li-Ion Battery Pack Equalization Control Strategy Research. *World Electr. Veh. J.* **2023**, *14*, 86. [[CrossRef](#)]
33. Singh, B.; Bist, V. An Improved Power Quality Based Sheppard–Taylor Converter Fed BLDC Motor Drive. *J. Inst. Eng. (India) Ser. B* **2014**, *96*, 327–337. [[CrossRef](#)]
34. Chitra, L.; Kumar, S.; Sarang, K.P.; Clinton, J. High Gain Sheppard Taylor Fed EV in a Grid Connected PV System. In Proceedings of the 2023 Third International Conference on Artificial Intelligence and Smart Energy (ICAIS), Coimbatore, India, 2–4 February 2023; IEEE: Piscataway, NJ, USA, 2023. [[CrossRef](#)]
35. Ang, S.; Oliva, A.; Griffiths, G.; Harrison, R. *Power-Switching Converters*; CRC Press: Boca Raton, FL, USA, 2010.
36. Shen, C.L.; Chen, L.Z.; Chen, H.Y. Dual-input isolated DC-DC converter with ultra-high step-up ability based on sheppard taylor circuit. *Electronics* **2019**, *8*, 1125. [[CrossRef](#)]
37. Huertas, J.L.; Mogro, A.E.; Jiménez, J.P. Configuration of Electric Vehicles for Specific Applications from a Holistic Perspective. *World Electr. Veh. J.* **2022**, *13*, 29. [[CrossRef](#)]

Disclaimer/Publisher’s Note: The statements, opinions and data contained in all publications are solely those of the individual author(s) and contributor(s) and not of MDPI and/or the editor(s). MDPI and/or the editor(s) disclaim responsibility for any injury to people or property resulting from any ideas, methods, instructions or products referred to in the content.